PAPER

Check for updates

Chitosan-coated halloysite nanotube magnetic microspheres for carcinogenic colorectal hemorrhage and liver laceration in albino rats

Sajid Majeed,[ab] Muhammad Qaiser,[af] Dure Shahwar,[a] Khalid Mahmood, [ID] *[b]
Nadeem Ahmed,[c] Muhammad Hanif, [ID] *[a] Ghulam Abbas,[d]
Muhammad Harris Shoaib, [ID] [e] Nabeela Ameer[a] and Muhammad Khalid[g]

Carcinogenic colorectal hemorrhage can cause severe blood loss and longitudinal ulcer, which ultimately become fatal if left untreated. The present study was aimed to formulate targeted release gemcitabine (GC)-containing magnetic microspheres (MM) of halloysite nanotubes (MHMG), chitosan (MCMG), and their combination (MHCMG). The preparation of MM by magnetism was confirmed by vibrating sample magnetometry (VSM), the molecular arrangement of NH_2, alumina, and silica groups was studied by X-ray diffraction (XRD) and energy-dispersive spectroscopy (EDS), the hollow spherical nature of the proposed MM was observed by scanning electron microscopy (SEM), functional groups were characterized by Fourier transform infrared (FTIR) spectroscopy and thermochemical modification was studied by thermogravimetric analysis (TGA). *In vitro* thrombus formation showed a decreasing trend of hemostatic time for MMs in the order of MHMG3 < MCMG3 < MHCMG7, which was confirmed by whole blood clotting kinetics. Interestingly, rat tail amputation and liver laceration showed 3 folds increased clotting efficiency of optimized MHCMG7 compared to that of control. *In vivo* histopathological studies and cell viability assays confirmed the regeneration of epithelial cells. The negligible systemic toxicity of MHCMG7, more than 90% entrapment of GC and high % release in alkaline medium made the proposed MM an excellent candidate for the control of hemorrhage in colorectal cancer. Conclusively, the healing of muscularis and improved recovery of the colon from granulomas ultimately improved the therapeutic effects of GC-containing MMs. The combination of both HNT and CTS microspheres made them more targeted.

1 Introduction

Colorectal cancer (CRC) is the 3rd most common cancer in men and 2nd most common cancer in women, with an increasing average of 10% per year across the world. The onset of CRC is strictly increasing due to aging, smoking, alcohol abuse, poor diet, diabetes mellitus, and increased body mass index (BMI). Treatments such as cancer chemotherapy immunotherapy, surgery, radiation, and target drug delivery are the only available options, but they still have many drawbacks with

[a]Department of Pharmaceutics, Faculty of Pharmacy, Bahauddin Zakariya University, Multan, Pakistan. E-mail: muhammad.hanif@bzu.edu.pk

[b]Institute of Chemical Sciences, Bahauddin Zakariya University, Multan, Pakistan. E-mail: khalidmahmood@bzu.edu.pk

[c]Center for Excellence in Molecular Biology, University of Punjab, Pakistan

[d]Faculty of Pharmacy, GOVT College University Faisalabad, Pakistan

[e]Faculty of Pharmacy, University of Karachi, Pakistan

[f]Drug Testing Laboratory, Punjab, Multan, Pakistan

[g]Department of Chemistry, Khwaja Fareed University of Engineering and Information Technology, Rahim Yar Khan, Pakistan

reoccurrence. Therefore, there is a necessity to develop a treatment that not only has a therapeutic effect against colorectal cancer but also equally effective in reducing colorectal hemorrhage.[1] The sustained effects of microspheres containing biodegradable polymers and their micro composites with clay-like minerals having ability to release a drug specifically in the colon make the MMs most suitable due to their increased surface area and pH-sensitive release.[2] Grafting magnetic microspheres with chitosan not only reduces their toxicity but also decreases the self-flocculation of magnetic microspheres.[3] The stability of dosage form, production process conditions, oxidation, hydrolysis, and the effect of gastrointestinal (GIT) pH are some limitations of simple microspheres, which can be overcome by preparing magnetic microspheres (MM). High mechanical resistance, ease of manufacturing, thermal stability, and excellent shelf life made MMs more targeted than simple microspheres.[4,5]

Halloysite nanotubes are effective as catalytic supports, pollutant adsorbents, and nanocarriers for functional compounds with biological and chemical activities because of their morphological properties.[6] The average length of

halloysite nanotubes (HNTs) is 2.01 m, and their inner and outer diameters, respectively, range from 6 to 60 nm and 30 to 160 nm. In this context, it is important to emphasize that halloysite is appropriate for biomedical and pharmaceutical applications due to its biocompatibility and low toxicity, which were seen in both unicellular and multicellular species.[7] The catalytic application,[8] drug release carrier,[7] and restoration properties[9] of HNTs were already reported in previous studies.

The problem of limited functional group binding of MMs was resolute by the addition of biodegradable polymers such as chitosan and halloysite nanotubes.[10] Chitosan (CTS) can be a possible option due to its strong chelating nature and ability to interact with various cross-linkers for microspheres preparation.[11] Biomedical polymers have the advantages of being degraded in the GIT, as already demonstrated, and additionally, they can protect colorectal anticancer drugs from the acidic pH. CTS and its complex with halloysite nanotubes (HNTs) can be used for the preparation of Ms. The HNTs have gained interest in nanotechnology applications due to their freely available and tubular structure. HNTs are negatively charged natural polymers having a tube or spherical sheet-like structure obtained from residues, and composed of inner alumina octahedrons and outer silicate tetrahedrons layers. MMs are constituted by the interaction of magnetic materials with natural and synthetic polymers. MMs are supramolecular particles with size less than 40 to 170 μm, and the ferromagnetic properties of the magnetic field, 0.5–0.8 tesla, can be a better option for the targeted release of colorectal cancer drugs.[12,13]

In our previous study, the CTS–HNT complex showed a positive response to control the clotting time.[14] As far as we are aware, there has not been any research done on the targeted release of gemcitabine (GC) for the treatment of colorectal cancer under the direction of the CTS–HNT magnetic complex that would have enhanced hemostatic qualities and more desirable cell regeneration potential. Colorectal cancer is the most advanced type of cancer worldwide. The mechanism of action of GC is to inhibit DNA synthesis as it is a nucleoside analog during the S-phase of the cell cycle. The GC is incorporated into DNA, and thus inhibits DNA replication in a cancerous cell. Moreover, it also promotes the apoptosis of cancerous cells.

Considering the foregoing work, the goal of the current work was to construct reproducible core/shell microspheres consisting of Fe_3O_4 with CTS and HNTs, loaded with GC. The application of the co-precipitation technique, analysis of magnetism, confirmation of thermodynamic surface characteristics, and hemostatic properties of the prepared MM made the study more interesting.[15,16] The size and zeta potential of the prepared microspheres were also measured, and their toxicity was determined using a cell viability assay. *In vitro* drug release profiles were characterized according to the drug loading and release procedure. In addition, the rat tail amputation and liver laceration activity of prepared MM and histopathological studies were also performed to confirm its uses for the targeted release of anticancer drugs in colorectal patients.

2. Materials and methods

2.1. Materials

Gemcitabine was provided by Novartis Pharma (Pvt.) Ltd Karachi. Halloysite nanotubes (MW ≈ 610.52 Da) with an average length of 2.01 μm, chitosan (MW ≈ 180–310 kDa), iron(III) hydrochloride hexahydrate ($FeCl_3 \cdot 6H_2O$, MW ≈ 270.195 Da), iron(II) hydrochloride tetrahydrate ($FeCl_2 \cdot 4H_2O$, MW ≈ 198.751 Da), 32% ammonia (MW ≈ 35.04 Da), Triton X-100, and 25 mM 4-(2-hydroxyethyl)-1-piperazineethanesulfonic acid (HEPES)-buffered saline of HPLC grade used for the cell viability studies were purchased from Sigma Aldrich, Germany. Glutaraldehyde (MW ≈ 100.11 Da) was purchased from BDH, UK; toluene, paraffin, span 80 (MW ≈ 1310 Da) as an emulsifier, petroleum ether (MW ≈ 82.2 Da), acetic acid (MW ≈ 60.052 Da), ethanol (MW ≈ 46.07 Da), methanol (MW ≈ 32.042 Da), *para*-phenylenediamine (PPD, 99.8%), sodium tetraborate, potassium dihydrogen phosphate (KH_2PO_4), sodium hydroxide, orthophosphoric acid, and a membrane filter (0.22–0.45 μm) were procured from Merck Darmstadt, Germany. Reverse osmosis, deionized, and double-distilled water were gifted by the Drugs Testing laboratory of Multan, Pakistan.

2.2. Methods

2.2.1. Magnetic microspheres (MM) with and without HNTs. A slight modification of the previously reported co-precipitation process was used for synthesis by Ma Dai *et al.*[17] Briefly, an aqueous suspension of $FeCl_3 \cdot 6H_2O$ and $FeCl_2 \cdot 4H_2O$ in a ratio of 2.4 : 1.0 was prepared at 60 °C in a controlled nitrogen environment. Ammonia solution (32%) was added dropwise after achieving the alkaline pH 9 with 1 M NaOH. The final mixture was heated at 70 °C for 4 h. This resulted in Fe_3O_4 microspheres, which were washed thrice with double-distilled water, dried at 60 °C in a vacuum oven, and stored in a well-sealed container for further use. A similar process was repeated with the addition of different concentrations of the preactivated HNT suspension (shown in Table 1) in the aqueous suspension of Fe_3O_4 and resulted in HNTs/Fe_3O_4 (MHM1 to MHM5) microspheres that were washed with water and stored in sealed containers.[18]

2.2.2. Chitosan MMs with and without HNTs. Chitosan (CTS) containing MM (CTS/Fe_3O_4) were prepared by an already reported method of E. Türkeş *et al.* with slight modifications.[19] Briefly, 2% m/v CTS solution in 2% acetic acid was added into 1 g of already prepared Fe_3O_4 microspheres (CTS/Fe_3O_4). A paraffin and span 80 (100 : 8, emulsifier) mixture was added into CTS/Fe_3O_4 with continuous stirring at 1500 rpm at 40 °C for 2 h. Finally, 25% glutaraldehyde saturated with toluene (GST) was added for crosslinking purposes with continuous stirring at 60 °C for 1 h. This resulted in CTS/Fe_3O_4 microspheres being centrifuged and washed with petroleum ether, ethanol, and distilled water respectively. Dried microspheres of CTS/Fe_3O_4 (MCM1 to MCM5) were stored in a well-sealed container for further use.[20] A similar procedure was used for the preparation of CTS/Fe_3O_4/HNTs with the addition of HNTs (MHM1 to MHM5) and a combination of both CTS and HNTs (MHCM1 to

Paper

Table 1 Different formulations of gemcitabine (GC) loaded magnetic microspheres (MM) with their physicochemical properties and TGA profile of 50 mg of each sample with RM (residual mass wt%), DM (degraded mass wt%) and LM (mass loss wt%) at 180 °C and 800 °C

Gemcitabine loaded MM	Formulation code	HNT (%)	CTS (%)	Fe_3O_4 microspheres (% yield) FeCl$_2$ & FeCl$_3$ (2.4 : 1)	Hausner's ratio	Gemcitabine loading (%)
HNTs/Fe$_3$O$_4$/GC	MHMG1	15	0	85	1.12 ± 0.01	49.90 ± 1.20
	MHMG2	17	0	83	1.10 ± 0.02	60.95 ± 1.06
	MHMG3	19	0	81	1.01 ± 0.03	72.24 ± 0.98
	MHMG4	21	0	79	1.02 ± 0.02	51.75 ± 0.94
	MHMG5	23	0	77	1.02 ± 0.01	65.46 ± 0.89
CTS/Fe$_3$O$_4$/GC	MCMG1	0	15	85	1.03 ± 0.01	40.25 ± 0.78
	MCMG2	0	17	83	1.02 ± 0.02	56.37 ± 0.96
	MCMG3	0	19	81	1.01 ± 0.02	65.21 ± 1.03
	MCMG4	0	21	79	1.02 ± 0.02	65.08 ± 0.97
	MCMG5	0	23	77	1.00 ± 0.01	70.71 ± 0.86
CTS/Fe$_3$O$_4$/HNTs/GC	MHCMG1	12	12	76	1.02 ± 0.02	44.20 ± 3.23
	MHCMG2	11	12	77	1.03 ± 0.01	55.57 ± 2.83
	MHCMG3	10	12	78	1.03 ± 0.01	56.46 ± 2.56
	MHCMG4	10	14	76	1.04 ± 0.02	57.08 ± 2.87
	MHCMG5	10	15	75	1.20 ± 0.02	65.97 ± 2.88
	MHCMG6	10	16	74	1.10 ± 0.01	75.54 ± 3.04
	MHCMG7	15	15	70	1.01 ± 0.02	90.34 ± 2.76
	MHCMG8	14	14	72	1.02 ± 0.01	80.14 ± 3.22
	MHCMG9	13	13	74	1.04 ± 0.02	79.93 ± 3.45

Thermogravimetric parameters

Materials	LM$_{180}$/wt%	RM$_{800}$/wt%	DM$_{800}$/wt%
MHMG3	05 ± 0.5	50 ± 0.5	45 ± 0.5
MCMG3	10 ± 0.5	35 ± 0.5	55 ± 0.5
MHCMG7	06 ± 0.5	10 ± 0.5	15 ± 0.5

MHCM9), as shown in Table 1. The % yield was calculated using eqn (1):

$$\% \text{ yield} = \frac{W_{mg}}{Wt_{mg}} \times 100 \tag{1}$$

"W_{mg}" is the weight of the CTS/HNTs microspheres and "wt_{mg}" is the weight of all contents used in preparation.

2.2.3. Physicochemical properties. Bulk density and tapped density of gemcitabine (GC)-unloaded HNTs/Fe$_3$O$_4$, CTS/Fe$_3$O$_4$, and CTS/Fe$_3$O$_4$/HNTs, and GC-loaded CTS/Fe$_3$O$_4$/GC, HNTs/Fe$_3$O$_4$/GC, and CTS/Fe$_3$O$_4$/HNTs/GC microspheres were calculated using a simple glass apparatus. Briefly, 1000 mg of all three types of MM were used for bulk and tapped densities, Carr's index, and angle of repose:

$$\text{Bulk density} = \frac{m}{V_b} \tag{2}$$

$$\text{Tapped density} = \frac{m}{V_t} \tag{3}$$

$$\text{Carr's index} = \frac{V_t - V_b}{V_b} \times 100 \tag{4}$$

$$\text{Hausner's ratio} = \rho_{tap}/\rho_b \tag{5}$$

$$\tan \varnothing = 2 \, h/d \tag{6}$$

where "m" is the powder mass in g, "V_b" and "V_t" are powder bulk volume and tapped volume in cm^{-3}, ρ_{tap} and ρ_{tap} are the tapped and bulk density, and h and d are the cone height and diameter of the powder heap respectively. For powder having good flow, Hausner's ratio should be less than 1.25.

2.2.4. Electromagnetic properties. The electromagnetic behaviors of MHM (1–5), MCM (1–5), MHCM (1–9), MHMG (1–5), MCMG (1–5), and MHCMG (1–9) microspheres were calculated using a vibrating sample magnetometer (7400 series). Briefly, 100 mg sample powder was placed in a Teflon sample holder and magnetic field 1 μ at 25 °C was applied and difference of magnetism among GC-loaded and GC-unloaded microspheres was observed using a cryogenic limited device (PPMS) of a vibrating sample magnetometer under 10 kOe magnetic fields at room temperature, providing a powerful investigation device having a capacity of low temperature 1 K to 7 tesla magnetic fields. Magnetic contents in the solution were assayed at 248 nm by AAS and % of contents can be calculated using eqn (2):

$$wt_\% = \frac{PPm(mg \, L^{-1}) \times \text{volume in mL} \times \text{dliution}}{\text{Weight of sample in grams}} \tag{7}$$

"PPm" is the result shown by the instrument and "mL" is the volume for digestion, and 100 mg weight of each sample was used.

2.2.5. Structural and techno-functional properties. The structure of all proposed microspheres and their components, *i.e.*, Fe_3O_4, CTS, and HNTs, with and without GC was confirmed by X-ray diffraction (XRD) studies. First, 100 mg samples were placed in a copper holder for their exposure to 40 mA × 40 kV radiation by using a wide-angle instrument (JDS 3525, Jeol Japan),[21] and differences in the peaks were observed. The thermal stability of all samples was investigated using a ZTY-ZP type thermal analyzer (model TGA Q500, Hullhorst, Germany). Briefly, 50 mg of each sample was used and heated from 50 to 800 °C with a temperature variation rate of 10 °C min^{-1} in an N_2 environment. The degraded mass was calculated using the following formula:

$$DM_{800}\ wt\% = 100 - (LM_{180}\ wt\% + RM_{800}\ wt\%) \tag{8}$$

where DM_{800} wt% is the degraded mass at 800 °C, LM_{180} wt% is the loss mass at 180 °C and RM_{800} wt% is the residual mass of samples at 800 °C respectively.[7]

Functionalization was confirmed using a diamond-based ATR-FTIR spectrometer (Bruker alpha, Germany). An average of 12 scans with 4 cm^{-1} resolution were calculated and the spectra ranging from 4000 to 400 cm^{-1} were reported at room temperature. Elemental and morphological analyses were performed using an energy-dispersive spectrometer (EDS; Jeol Japan) equipped with a detector model elemental analyzer (EX-541/5JMU), while the morphology was observed using a scanning electron microscope (SEM) (Jeol Japan detector, JSM-6380A). The samples were placed in an aluminum mount, with adhesive on both sides, and carbon tape was used for electrical conductivity. Palladium and gold (40 : 60%) were used as coating materials for 30 s and 48 mA current with 38 kV voltage and an average of three experiments was reported.[20]

2.2.6. Size and surface charge characterization. The size of all microspheres was analyzed by the already reported method of Liu M. *et al.*,[27] using Zetasizer Nano-z (Malvern Instrument Ltd., Worcestershire, UK) with disposable folded capillary cells. Briefly, a dispersion of 10 mg sample in 1 mL distilled water was prepared, vertexed at room temperature and mean diameter and size distribution of the prepared microspheres were measured by dynamic light scattering at 633 nm at 36 ± 0.5 °C. The effect of different pH conditions on zeta potential changes of prepared microspheres was measured by the method reported by Hosseinzadeh H. *et al.*[51] Then, 10 mg mL^{-1} suspension of all formulations were prepared in 0.1 M (HCL) having pH 1.2 and 50 mM phosphate buffer having pH 4.5, 6.0, 6.8 and 7.4. Zeta potential changes were measured and each experiment was repeated thrice for average results.[22]

A light microscope was used to keep track of the microsphere suspension's condition (LM; model Axioscope A1, Carl Zeiss Microscopy GmbH, Jena, Germany). Important characteristics of interest included microsphere morphology (such as size) and a propensity to exist in a liquid media. Additionally, the light microscope was utilized to see how microspheres' size altered throughout wet milling.[23] The morphological study using optical microscopy was done to determine how the microspheres' size and shape related to one another. The microscopy photos display spherical particles with what appears to be internal granulation, and they also demonstrated homogeneity in terms of morphology among many microsphere components. The optical microscopic image of a single agglomerated particle of powder material with an optical spectrum showed the distribution of elements over the particle area.[24]

2.2.7. Cell viability studies. Cell viability studies of the prepared $CTS/Fe_3O_4/HNTs/GC$ (MHCMG7) microspheres were performed using the resazurin assay technique by already reported of S. Anoopkumar-Dukie *et al.*[25] Briefly, Caco-2 cells were seeded in a 24-well plate at a density of 25 000 cells/well cultured under the controlled conditions of 95% relative humidity and 5% CO_2 at 37 °C for 14 days. Old MEM was replaced with fresh MEM every 48 h. MEM interference was minimized with Fetal Bovine Serum (FBS). Incubated cells were assayed by HEPES buffered saline (HBS) at pH 7.4 (25 mM). Freshly prepared 0.5 and 1% suspensions of MHCMG7 microspheres were replaced with already present white MEM. Microspheres containing wells were gestated, for 3 and 24 h under the controlled condition of relative humidity and CO_2. Fresh MEM and 0.2% Triton X-100 were used as positive and negative controls respectively. Then, 250 µL 2.2 mM resazurin solution was added in pre-washed cells containing fresh HBS buffer at 37 °C for 3 h. Fluorescence and metabolism of resazurin in Caco-2 cells were observed at 540 and 590 nm and fluorescence was observed by M200 Tecan Infinite Grading, Austria. A similar procedure was repeated for 24 h incubation samples. The following equation was used for the calculation of toxicity:

$$Cell\ viability = \frac{absorbance\ of\ samples}{absorbance\ of\ standard} \times 100 \tag{9}$$

2.2.8. Processing variables and *in vitro* study. Optimized formulations from MHM, MCM, and MHCM microspheres were selected for loading the drug (GC). Approximately 50 mg microspheres were immersed with 1 mg mL^{-1} aqueous solution of GC with continuous stirring at 90 rpm for 24 h.[26] The concentration of GC from a microsphere-containing suspension was measured at different time intervals at 269 nm. The percentage released of GC was calculated in 100 mM phosphate buffers of pH 5.2, 6.8, and 7.4 at 37 °C using a USP II paddle apparatus (Erweka, Darmstadt Germany). The filtered supernatant of 1 mL was collected at predetermined time points, the same volume was replaced with a fresh medium and the concentration of GC was calculated at 269 nm. Drug release results were elaborated and understood by different kinetics models such as Korsmeyer–Peppas, Higuchi, first-order, and zero-order:

$$F = K_0 \times t \tag{10}$$

$$\ln(1 - F) = -K_1\ t \tag{11}$$

$$F = K_h \times t_{1/2} \tag{12}$$

$$Mt/M\infty = K_3\,t^n \qquad (13)$$

where K_0, K_1, K_h, and K_3 are zero-order, first-order, Higuchi dissolution and Korsmeyer–Peppas rate constants respectively. t is the time and n is the release exponent. The dissolution efficiency was measured by ratio of % age of the area under dissolution curve concerning time from 0 to 100% of area of the rectangle. The % GC loading, entrapment efficiency (EE), cumulative percentage release, and dissolution efficiency were calculated using eqn (9)–(12), respectively.

$$\text{Drug loading}(\%) = \frac{\text{Weight of drug in sample}}{\text{Weight of sample}} \times 100 \qquad (14)$$

$$\text{Entrapmet efficiency}(\%) = \frac{\text{Weight of drug in sample}}{\text{Theoretical weight of sample}} \times 100 \qquad (15)$$

$$\text{GC cumulative release}(\%) = \frac{\text{Amount of drug release}}{\text{Initial amount of drug Loaded}} \times 100 \qquad (16)$$

$$\text{Dissolution efficiency(DE)} = \frac{(\text{AUC})_o^T}{Q100T} \times 100 \qquad (17)$$

$(\text{AUC})_o^T$ and $Q100T$ are area under the curve and rectangle with 100% dissolution values measured.

2.2.9. *In vitro* thrombin, prothrombin, and thrombus formation. The hemostatic activity of optimized formulations, *i.e.*, MHMG3, MCMG3, and MHCMG7MM, was studied by the method already reported by Chenglong *et al.*[1] Briefly, five different groups of 10 mL blood samples were used in such a way that group 1 was considered false positive without treatment, and the remaining four were treated with MHMG3, MCMG3, and MHCMG7MM. Then, 3.2% m/v sodium citrate was added to the sample blood and centrifuged at 2000 rpm at 4 °C for 30 min and aPTT (activated partial thromboplastin time) reagent was mixed in a ratio of 1 : 1 and incubated at 37 °C for 15 min. The mixture was added in a test tube containing 25 mM $CaCl_2$ (used for recalcification) and the calculated amount of prepared microspheres. The coagulation time in seconds was observed in aPTT using a stopwatch. The same procedure was repeated for the calculation of the prothrombin test (PTT). The thrombin effect of MHMG3, MCMG3, and MHCMG7 microspheres was measured with 3.2% citrated fresh rat blood by the method reported by Sun *et al.*,[22] with slight modifications. Five groups for test samples were made. Each group has four glass tubes, and 0.5 mL, 3.2% sodium citrated fresh blood diluted with 10 mL deionized water was added in each glass tube to start thrombus formation. This resulted in the thrombus being soaked in a 37% formaldehyde solution for 15 min at 25 °C and dried at 50 °C for constant weight.

2.2.10. Stability study of MHCMG7. Stability studies of MHCMG7 were carried out in acidic and alkaline media under controlled conditions of room temperature and relative humidity conditions according to the ICH guidelines, and the estimated shelf life was determined using Rgui software.

2.2.11. Rat liver laceration and tail amputation test. The hemostatic effect of MCMG3, MHMG3, and MHCMG7 was evaluated by *in vivo* rat liver laceration and rat tail amputation experiments according to animal guidelines of the Ethical Committee of Baha Uddin Zakariya University, Multan, and ARRIVE animal guidelines.[28] For this purpose, adult rats ($n = 6$) with an average weight of 174 ± 5 g were anesthetized by keeping them in a chloroform jar for 2 to 3 min. The rat's chest was cut with a 1 cm × 0.5 cm deep incision in the right lobe of the liver, the sample of 0.2 g MHMG3 was instantly placed over the incised area, and then the incision was pressed with medical gauze until the bleeding stops. The blood over the sterile medical gauze was weighed using a precision balance (Mettler Toledo). Meanwhile, the same procedure was repeated for MHMG3 and MHCMG7. Rat without any sample was treated as blank.[29]

The rat tail was cut 1 cm from the tip. The first drop of blood should be discarded using sterile medical gauze. A pre-weighed sample of MCMG3 was administered at the cut site, and blood was poured over the gauze. The spilled blood was absorbed with medical gauze every 20 s. To assess the actual amount of blood loss, the amount of blood in grams was measured until the bleeding stopped and compared to the control. Meanwhile, the same procedure was repeated for MHMG3 and MHCMG7. Rat without treatment was treated as blank.[30]

2.2.12. Histopathological examination of rabbit's colon. Albino rabbits (1 to 1.5 kg) were divided into 5 groups as control (group 1), MHMG3 (group 2), MCMG3 (group 3), MHCMG7 (group 4), and GC market available brand® (group 5) with an equal number (12 in each group). Then, 24 h fasted rabbits were used for cancer induction. Cancer was induced by ingesting 30 mg kg^{-1} dimethylhydrazine once a week for 4–6 weeks. Dimethylhydrazine cause hyperplasia of intestinal mucosa resulting in severe granulomas in the colon.[31] Two rabbits of all groups were sacrificed, dissected, and removed from colon and formation of cancer cells was examined. The number of aberrant crypt foci (ACF) per cm^2, granulomas (G), and crypt abscesses (CA) were measured after a different period and found a rapid decrease in ACF per cm^2 before and after the administration of MHCMG7. Histopathological studies showed cancer development in the colon mucosa of control group as compared to the normal control group.[32]

2.2.13. Statistical analysis. All the results are interpreted using Microsoft Excel and GraphPad. To select the optimized formulations of CTS, HNTs, and CTS/HNTs MM, and to study the effects of variables, ANOVA was used ($p < 0.05$).

3. Results and discussion

In this work, the phenomenon of magnetism was investigated for colon-targeted delivery of GC. MM are supramolecular particles that can flow through capillaries without obstructing them when a magnetic field of between 0.5 and 0.8 tesla was applied. However, they are also sufficiently prone to being caught in microscopic arteries and drawn into adjacent tissues.
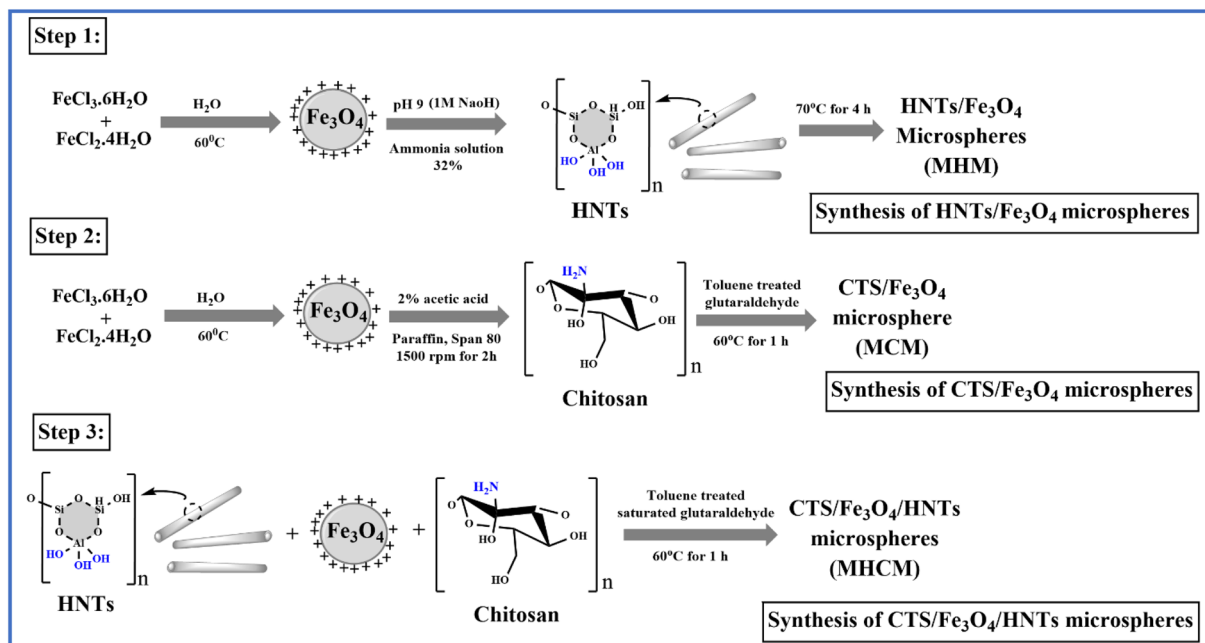
Fig. 1 Chemical scheme for the synthesis of microspheres (MHM, MCM, and MHCM), (step 1) synthesis of HNT magnetic microspheres (MHM) in the presence of an ammonia solution, (step 2) synthesis of CTS magnetic microspheres (MCM) in the presence of toluene-saturated glutaraldehyde (TSG), and (step 3) synthesis of CTS and HNT magnetic microspheres (MHCM) with TSG.
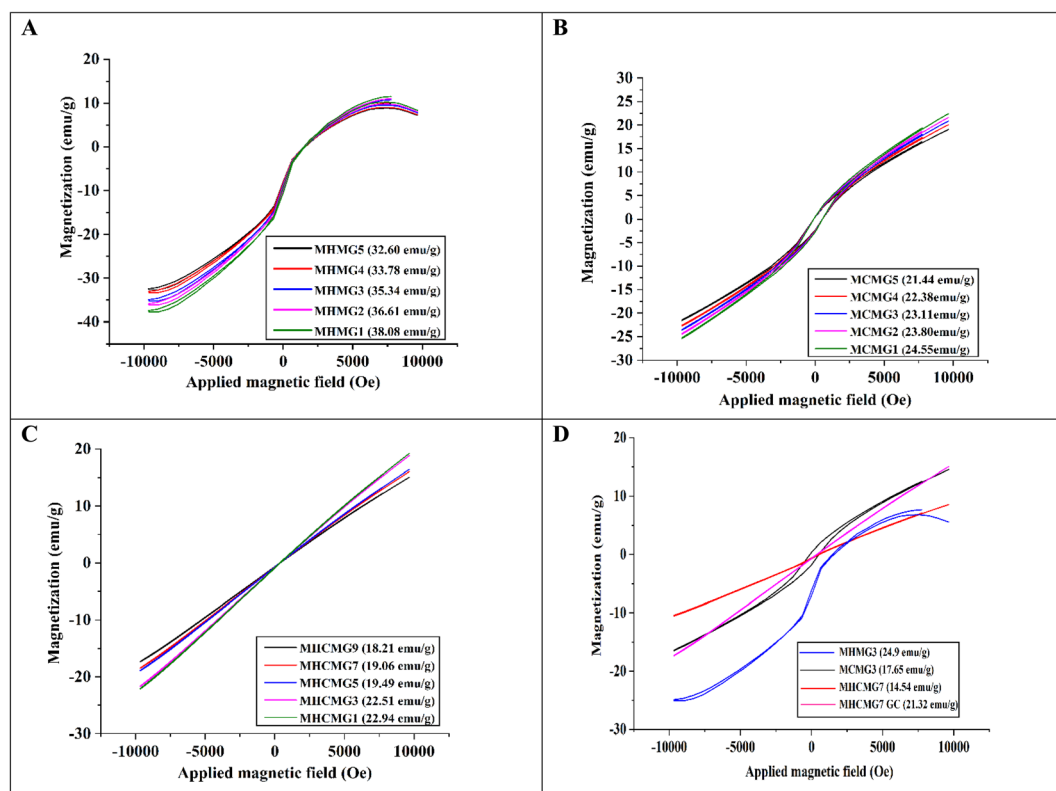

Fig. 2 VSM analyses of different MM (A) HNTs/Fe_3O_4 (MHMG1 to MHMG5), (B) CTS/Fe_3O_4 (MCMG1 to MCMG5) (C) CTS/Fe_3O_4/HNTs (MHCMG1 to MHCMG9), and (D) comparative VSM analysis of optimized formulation MCMG3, MHMG3, MHCMG7 and MHCMG7 GC (gemcitabine loaded) microspheres.

MM of CTS and HNTs were prepared by a solvent emulsion evaporation technique using TSG as a cross-linker. In Fig. 1, a chemical scheme for materials is proposed. According to step 1, Fe_3O_4 was dissolved in 32% ammonia solution whose pH was adjusted to 9 with a 1 M NaOH solution. Meanwhile, MHM was prepared after adding HNTs to the prepared solution at 70 °C under stirring for 4 h. According to step 2, Fe_3O_4, paraffin, and span 80 were dispersed in a 2% acetic acid solution at 1500 rpm for 2 h. Meanwhile, MCM was prepared after adding CTS into prepared solution in the presence of toluene-saturated glutaraldehyde (TSG) at 60 °C, while MHCM was prepared by a similar method that is reported in step 2. The resulting MHCM was washed with ethanol and distilled water.

All types of MM showed excellent flow, which was confirmed by Hausner's ratio, Carr's index, and the angle of repose acceptable values. Hausner's ratio was 1.01 ± 0.03, 1.01 ± 0.02 and 1.01 ± 0.02, Carr's index was 10 ± 2, 12 ± 2 and 11 ± 2, and the angle of repose was 18 ± 0.5, 19 ± 0.5 and 17 ± 0.5 of the optimized formulation *i.e.*, MHMG3, MCMG3, and MHCMG7, respectively. The percentage yield of unloaded MM was in between the range of $39.19 \pm 2.18\%$ to $43.84 \pm 2.01\%$ while the loading of GC was 89.14 ± 2.17 to $93.62 \pm 2.17\%$, which was

confirmed by an already constructed standard curve of increasing concentration of pure GC at 269 nm. MHM3 and MHMG3 showed the highest bulk density, lowest tapped density, decreased Carr's index, and increased angle of repose due to the cylindrical shapes of HNTs, which created wide spaces among the microspheres. MHMG3 was an optimized formulation among the HNT-containing MM due to its maximum percentage loading and dominant hollow structure. In the case of MCMG3, the presence of CTS made the significant loading of GC due to its spherical and pH-dependent nature. Finally, the combined HNT- and CTS-containing MHCMG7 have both properties of the hallowed nature and positive charge at a lower pH providing a percentage loading of $90.34 \pm 2.76\%$.[33] The comparative results of the tapped density of optimized MHCM7-unloaded and GC-loaded microspheres were 0.64 ± 0.02 g cm^{-3} and 0.92 ± 0.06 g cm^{-3}, respectively. The increase in tapped density may be due to the higher molecular weight of GC, which increased the mass of resulting microspheres and decreased wide space among the particles. The increased value of Carr's index and the decreased value of the angle of repose of the optimized formulation having both HNTs and CTS may be due to the overlapping of CTS on the surface of HNTs, which
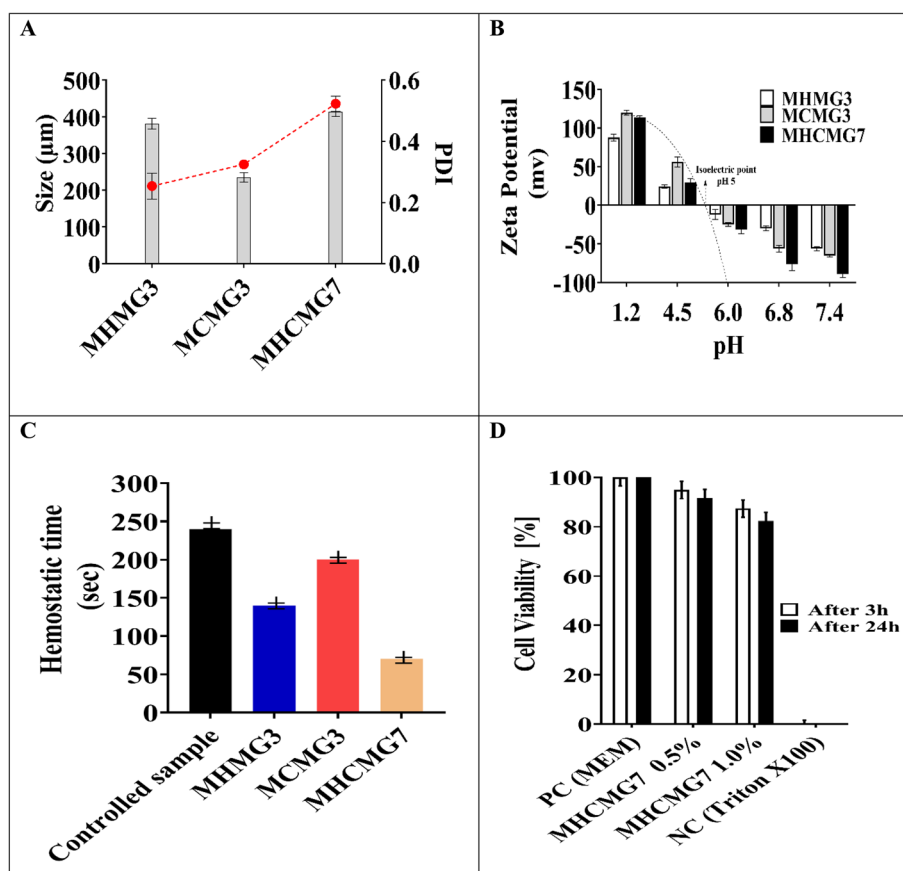

Fig. 3 (A) Zetasizer particle size of MHMG3, MCMG3, and MHCMG7 microspheres was calculated and reduction in particle size confirmed the formation of the complex. (B) Zeta potential and ion pairing changes were observed and a positive charge was found in an acidic medium, which converted into a negative charge in an alkaline buffer at pH 6, 6.8, and 7.4. (C) Hemostatic effect of MHMG3, MCMG3, and MHCMG7, which shows 2.5 folds increase in thrombin formation of MHCMG7. (D) Cell viability and metabolic activity were observed from 100% to 0% at pH 7.4 for 3 h and 24 h, PC; positive control and NC; negative control, respectively.

made them smooth. Excellent flow properties of the optimized microspheres were further used for the oral drug delivery system, which can release GC in the colon and is more targeted for the treatment of colorectal cancer.[33]

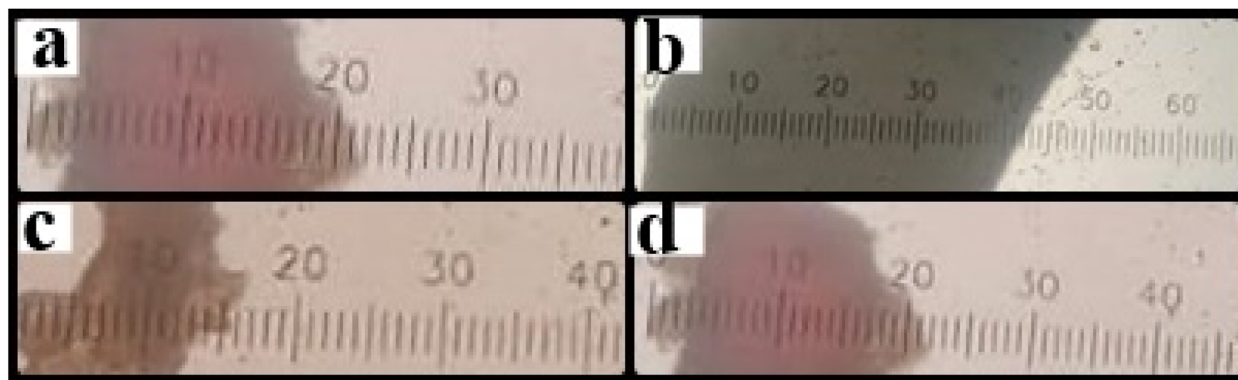### 3.1. Electromagnetism of microspheres

Fig. 2(A)–(C) shows the VSM analyses of GC-loaded HNT-containing MHMG (1 to 5), CTS-containing MCMG (1 to 5), and both HNT- and CTS-containing MHCMG (1 to 9) microspheres. The hysteresis curves obtained for MHMG showed the function of the magnetic field applied at room temperature with superparamagnetic properties. Magnetization and values of HNT-containing microspheres ranged from 14.07 to 25.35 emu g^{-1}, which may be due to concentration difference between HNTs and GC.[34] A decrease in magnetization was observed by increasing the concentration of HNTs due to overlapping of HNTs on Fe_3O_4. Fig. 2(B) shows a slight decrease in magnetization of CTS-containing MCMG from 20.32 to 16.79 emu g^{-1}, which was attributed to the formation of complete spherical shapes of microspheres. In the case of MHCMG, the increased values of magnetization may be due to the complete interaction of negatively charged HNTs and positively charged CTS, which ultimately frees the availability of Fe_3O_4 for magnetization. The loading of GC into MM has very little effect on magnetization. The magnetization curve showed a small hysteresis loop and a slight coercivity as a typical characteristic of magnetization and the remanence values approach zero. It was scrutinized that the increase in HNT concentrations in MHM microspheres had superparamagnetic properties. MHCMG (1 to 9) microsphere magnetization ranged from 22.54 to 25.35 emu g^{-1}, respectively as shown in Fig. 2(A). Optimized formulation MHCMG7 microspheres showed maximum magnetization values of 25.35 emu g^{-1} and were excellent candidates for controlled release of GC-like drugs on targeted sites, as shown in Fig. 2(D).[35]

3.2. Size and surface charge studies

Fig. 3(A) shows the effect of different concentrations of polymers and temperature conditions of HNT, CTS, and both CTS GC-containing MHMG3, MCMG3, and MHCMG7 respectively.[36] The size of the HNT-containing microspheres was 135 ± 5.91 to 157 ± 5.86 μm, while in the case of CTS-containing microspheres, it also increased from 123 ± 6.56 μm to 140 ± 6.97 with a PDI value less than 0.5. The decrease in the size of MCMG3 as compared to MHMG3 may be due to the formation of complete complexes in the form of covalent bond of chitosan on the outer surface of Fe_3O_4. In case of combined HNTs and CTS, MHCMG7 showed further increase in the particle size from 50 to 70 μm with PDI values of 0.453, which may be due to cross-linking of HNTs with chitosan in the presence of TSG making them excellent for the targeted release of anticancer

Table 2 Size determination of microspheres *i.e.*, MHMG3, MCMG3, and MHCMG7 using optical microscopy, part a and b showed results before milling while c and d showed results with size reduction after milling

Before milling (Y^-, 190.5 μm)

Sample	Diameter X (μm)	Y = X CF	$(X - Y^-)^2$	$SD = \sqrt{(X - Y^-)^2/n}$
MHMG3	29	130.5	2682.22	161.49
MCMG3	56	252.4	18090.25	134.55
MHCMG7	42	189.2	22052.25	148.56
After milling (Y^-, 84 μm)				
MHMG3	22	99.3	3844	62.32
MCMG3	16	72.2	4624	68.35
MCMG7	18	81.4	4356	66.66

© 2023 The Author(s). Published by the Royal Society of Chemistry

drugs.[37,38] Zeta potential changes of all formulations are reported in Fig. 3(B), the positive charge in all formulations was observed in acidic environments, *i.e.*, from pH 1.2 to 4.5, while the negative behavior in alkaline media is attributed to the enhanced permeation of GC from negative charge-carrying mucous membrane.[39,40] The presence of CTS in MCMG3 formulations showed the highest changes in the acidic medium as compared to HNT-containing MHMG3 and MHCMG7, which may be due to the presence of an amino group with a positive charge. In the case of alkaline pH, MHCMG7 formulations had the highest values of zeta potential attributed to the formation of complete sphere complexes, which made them an excellent candidate for the release of anticancer drugs in an alkaline medium like colon.[40] Table 2 shows the optical microscopic image of the microspheres dispersed in distilled water.[41] These results indicated the morphological and size changes before milling of microspheres, *i.e.*, 190.5 μm of MHCMG7, while after milling, the size of microspheres reduced to about 84 μm.[42]

3.3. Structural and techno-functional properties

Fig. 4(A) presents the X-ray diffraction patterns of GC-loaded MHMG, MCMG, and MHCMG microspheres, and distinct peaks were observed. The diffraction line of MHMG3 at 15.89° (2θ) and MCMG3 at 19.59° (2θ) showed the crystalline nature of the reported microspheres. The presence of HNTs decreased the 2θ values, while inverse was observed in case of CTS, *i.e.*, 15.89

to 19.5. Furthermore, characteristic distinct peaks at 2θ values were observed at 17.59°, 24.41°, 25.03°, 26.89°, 27.15° and 28.74° for MCMG (1 to 5), while they were slightly shifted by increasing Fe_3O_4. The diffractogram peak of MHCMG7 at 7.85°, and 18.69° (2θ) and GC-loaded MHCMG7 were observed at 14.47°, 19.58°, 20.95°, 24.31°, 26.03°, 36.15° and 38.56° (2θ), respectively. The diffraction peak of CTS disappeared in the XRD pattern of MHCM3 and MHCMG7 microspheres due to entrapment of Fe_3O_4 in CTS microspheres. The relative peak intensities and peak position indicated the successful introduction of CTS, HNTs, and GC into Fe_3O_4 microspheres.[43]

Fig. 4(B) shows the TGA and weight loss of MHMG3, MCMG3, and MHCMG7. Rapid weight loss during heating from 30 to 180 °C of all the formulations was observed due to presence of water molecules in the compositions. Stability in the weight loss was observed from 180 to 300 °C due to formation of stable structures among HNTs and Fe_3O_4 in the case of MHMG3, while CTS and Fe_3O_4 in MCMG3. The sudden decrease in weight loss was started after 220 °C in case of MHCMG7, and two peaks at 225 °C and 480 °C were observed showing the decomposition of covalent bonds between HNTs and CTS. Finally, at 550 °C, complete decomposition of MHCMG7 was observed attributed to the stability of GC-loaded microspheres, which made them more acceptable for drug-loaded purposes. Fig. 4(C) shows the DTG analysis results of all prepared microspheres, supported by TGA results.[44] The initial water loss of all samples was observed in DTG peaks at a temperature of 180 °C. The initial large peak at 66 °C and 510 °C in MHCMG7 was due to denaturation. The
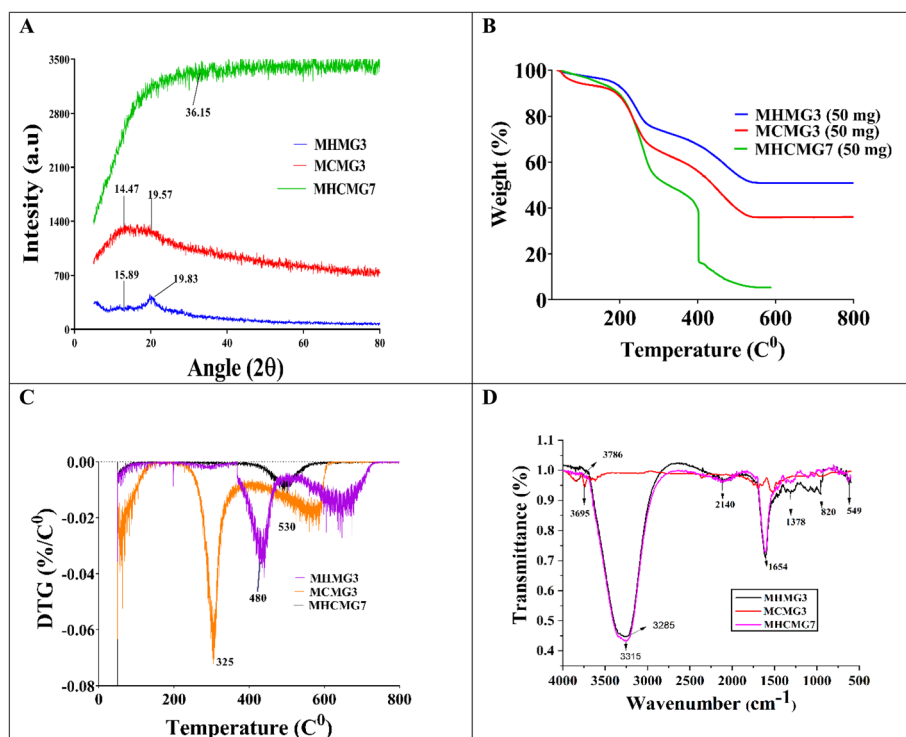

Fig. 4 Analysis of gemcitabine–loaded and -unloaded different MMs: (A) XRD analysis define the diffraction line ranging from 14.47° (2θ) to 26.31° (2θ). (B) TGA analysis showing the rapid weight loss during heating from 30 to 170 °C and a further decrease at 220 °C. Complete denaturation magnetic microspheres observed before 600 °C. (C) DTG at 225 °C and 480 °C, MCMG3 at 260 °C and 415 °C, MHMG3 61 °C, 280 °C and 530 °C and drug loading MHCMG7 at 66 °C and 510 °C. (D) FTIR analysis results.

complete decomposition of organic chitosan and structure loss was observed at 180–400 °C. However, significant reduction in weight loss of organic compounds may be due to the stable structure of HNTs. Other factors such as de-hydroxylation of $Al(OH)_3$ in HNTs made the complex more stable at a temperature between 400 and 500 °C.[43]
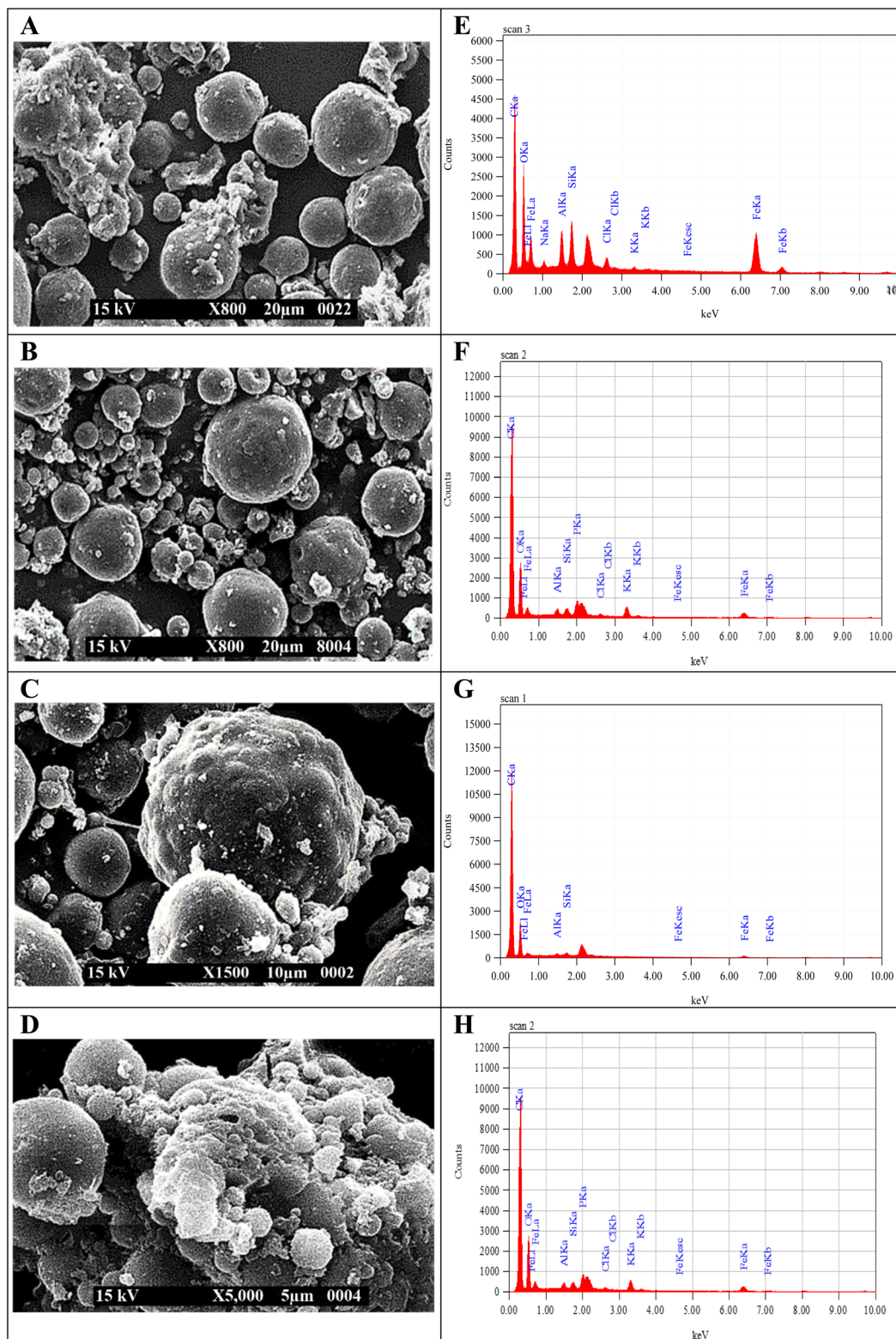

Fig. 5 SEM analysis of MHMG3 (A), MCMG7 (B) MHCMG7 (C), and drug loading MHCMG7. (D) EDS analysis of MHM3 (E), MCMG7 (F) MHCMG7 (G), and drug loading MHCMG7 (H).

Fig. 4(D) briefly describes the FTIR spectra in the 4000–40^0 cm^{-1} wavenumber range of MHMG3, MCMG3, and MHCMG7 microspheres. HNTs show peaks at 911 cm^{-1} and 3695 cm^{-1} due to the deformation and stretching of the O–H group respectively.[45] Two peaks of HNTs were observed at 1121 cm^{-1} and 756 cm^{-1} due to Si–O group stretching. Chitosan spectra at peaks of 1039 cm^{-1}, 3400 cm^{-1}, 1680 cm^{-1}, 1180 cm^{-1}, and 820 cm^{-1} were due to the C=C stretching vibration (CH$_3$OH), NH stretching, C=O, and C–O group stretching respectively. Slight shifts in NH bending from 1556 cm^{-1} to 1552 cm^{-1} were observed due to cross-linking with glutaraldehyde. A new absorption peak was observed at 1656 cm^{-1}, indicating the formation of (C=N) by CTS and glutaraldehyde. The absorption peak at 3716 cm^{-1} and 3786 cm^{-1} is related to Al(OH)$_2$ stretching. Two peaks at 967 cm^{-1} and 1115 cm^{-1} were assigned to Si–O and O–H group deformation. The incorporation of HNTs was confirmed by an absorption band at 543 cm^{-1} due to the deformation of Al–O–Si, and bands at 3673 cm^{-1} and 3714 cm^{-1} were attributed to O–H stretching of HNTs. A slight shift of 549 cm^{-1}, 3691 cm^{-1} and 3720 cm^{-1} was observed after HNT incorporation.[46] All the above-mentioned characteristic spectra of Fe$_3$O$_4$, HNTs, CTS, and GC confirmed successful incorporation into MHMG3, MCMG3, and MHCMG7 microspheres. The absorption spectra of GC were observed at 2936 cm^{-1} due to CH$_2$ stretching, and at 1681 cm^{-1}, and 1061 cm^{-1} due to stretching of the C–O group. The absorption peak was observed at 1757 cm^{-1} due to the uredo group in GC. The formation of a broadband at 3050–3600 cm^{-1} was due to strong hydrogen bond between GC and MCMG3.[46,47]

Fig. 5(A)–(D) confirm that the spherical shape of MMs becomes irregular or wrinkled during observation due to the shrinkage of particles upon drying.[43] The presence of the *N*-acetyl glucosamine group in CTS molecules made their shape irregular as the concentrations of CTS increased in CTS/Fe$_3$O$_4$, CTS (25%)/Fe$_3$O$_4$, and CTS (50%)/Fe$_3$O$_4$. The halloysite nanotubes were porous interior hybrid microspheres that overlapped loosely together. Many stripes were noted to form on the surface of the MHCMG7 microspheres.[48] The uneven surface of MCMG3 microspheres was reported due to the absorption of MHMG3 on the surface. A smooth surface of simple and CTS-containing Fe$_3$O$_4$ microspheres turned slightly rough after the addition of an increasing concentration of HNTs from HNTs/Fe$_3$O$_4$, HNTs (25%)/Fe$_3$O$_4$, and HNTs (50%)/Fe$_3$O$_4$. Change in the surface and formation of many strips on the surface may be due to the tube-like structure of HNTs. The sphericity of the MM becomes worse with higher HNTs. Loose overlapped structure and large surface area were favorable for drug loading into MHCMG7.[17]

Fig. 5(E)–(H) shows the elemental analysis of MHMG3, MCMG3, MHCMG7 (without drug loading), and MHCMG7 (drug-loaded). The presence of iron, oxygen, carbon, potassium, chlorine, sodium, aluminum, and silicon was determined and compared.[48,49] The increasing ratio of carbon and oxygen was in the order of MCMG3 > MHMG3 > MHCMG7 microspheres, while chlorine and potassium were only observed in MHMG3 microspheres, which may be due to HNTs. The Al and Fe ratio decreased with the addition of HNTs and CTS due to their complex formation with Fe$_3$O$_4$.[43,45]
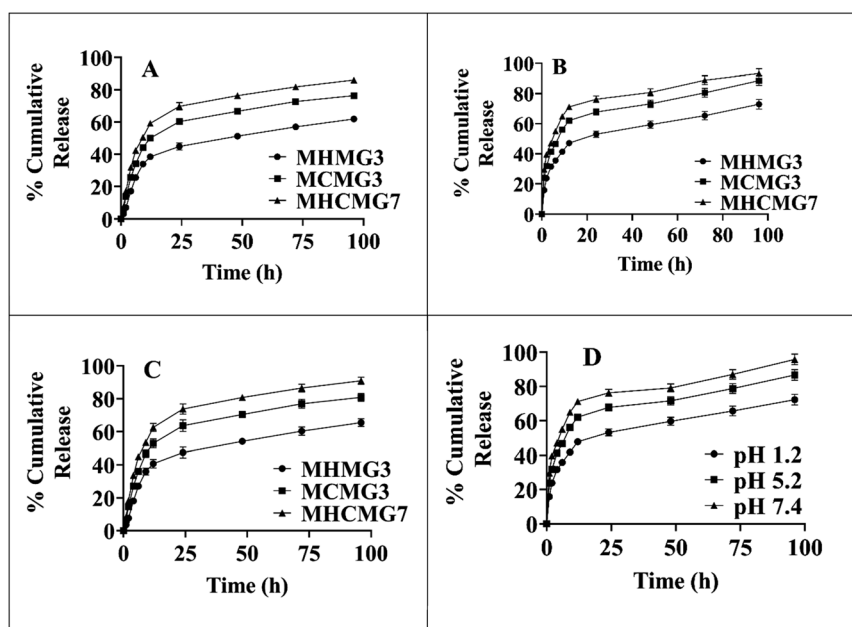

Fig. 6 (A) Gemcitabine-loaded MMs, *i.e.*, MCMG3, MHMG3, and MHCMG7 showing cumulative percentage release of 72.28%, 86.67%, and 95.78% after 96 h at pH 7.4 respectively. (B) Gemcitabine-loaded MMs of MCMG3, MHMG3, and MHCMG7 showing cumulative percentage release of 65.53%, 80.84%, and 90.98% after 96 h at pH 5.2 respectively. (C) Gemcitabine-loaded microspheres of MCMG3, MHMG3, and MHCMG7 showing cumulative percentage release of 53.26%, 59.77%, and 66.59% after 96 h at pH 1.2 respectively. (D) Cumulative percentage release of gemcitabine-loaded MHCMG7 microspheres at different pH values.

3.4. Processing variables and *in vitro* studies

Fig. 6 shows the percentage release of GC from MHMG3, MCMG3, and MHCMG7 at acidic as well alkaline pH 1.2, 5.2, and 7.4, respectively. All formulations showed a maximum percentage release at 7.4 due to the presence of chitosan. There is no chemical interaction between GC and CTS. GC was physically loaded in MHMG3, MCMG3, and MHCMG7. The pH-dependent nature of CTS with GC was already reported in the literature. At a low pH, CHT-free NH_2 groups were charged, causing the repulsion of polymer chains. This will result in the controlled release of GC.[38] NH_2 groups of CTS-containing formulations were protonated at a slightly acidic pH, while presence of HNTs provided the favorable controlled percentage release of GC at an alkaline pH due to their electrostatic repulsion and drug loading in the HNT lumen,[50] as shown in Table 1. The first burst release, *i.e.*, 45% of GC from MHCMG7 microspheres within 6 h at pH 7.4 confirmed the presence of GC at the surface of optimized microspheres. After 96 h, more than 80% of GC release at pH 7.4 confirmed the sustained release behavior of GC, which made the formulation ideal for the treatment of colorectal cancer.[51] In Fig. 7, the stability of optimized MHCMG7 was calculated according to Rgui and the estimated shelf life was 30 months.

3.5. Plasma coagulation

Table 3 shows the comparison of all formulations of GC-loaded MM. The maximum hemostatic effect of MHCMG7 as compared

Fig. 7 Stability study and estimated shelf life of MHCMG7.

to MHMG3 and MCMG3 was observed due to the formation of CTS and HNT complexes, as shown in Fig. 3(C). The results indicated that the MM reduces the time for aggregation of not only erythrocytes but also platelets. The clotting time of control (without treatment) was 232 ± 6.08 s, which was reduced to 220 ± 5.93 s in the case of MHMG3. MCMG3 clotted the blood in 140 ± 6.08 s, which was further reduced to 89 ± 7.13 s by using MHCMG7. Similar behavior of whole blood clotting was observed by Sun *et al.*[22] The thrombogenic activity of all microspheres was significantly shorter than the control sample, which may be due to the formation of intrinsic blood coagulation (fibrin formation), and their interaction with negatively charged HNTs. The weight of the whole blood clot was 82 ± 5.08, 100 ± 4.99, 194 ± 5.99, and 216 ± 5.04 mg for control, MHMG3, MCMG3, and MHCMG7, respectively. An increase in the clotted blood weight and roughness of the beads' surface (clotted blood) was observed by using the optimized MHCMG7 due to rapid interaction of the positively charged amino group with negatively charged RBCs. Eventually, rapid clotting process of optimized MHCMG7 made the formulation excellent for the control of hemorrhage process in the case of colorectal cancer patients.

3.6. Rat liver laceration and tail amputation test

Under ARRIVE animal guidelines,[52] which were approved by the Animal Ethics Committee of Baha Uddin Zakariya University, hemostatic assays were carried out on the rat tail and rat liver.[28] Fig. 8 and Table 4 showed that the bleeding volume and bleeding time were significant parameters. Due to more effective blood coagulation caused by the positive surface charge of CTS, bleeding duration in case of MCMG3 was dramatically reduced by 1.5 folds as compared to the control. Due to epithelial regeneration and higher collagen deposition at the damaged region, MHMG3 demonstrated only a 0.8-fold increase in efficiency compared to the control.[27] Interestingly, MHCMG7 demonstrated three times greater hemostatic effectiveness because of the interaction between HNTs and CHT MM. The bleeding volume and bleeding duration were found to be 0.03 g and 15 s, respectively, as opposed to that of the control, 3.33 ± 0.03 g and 290 s.

Rats ($n = 6$) were used to investigate the hemostatic effectiveness of MCMG3, MHMG3, and MHCMG7 using a tail amputation procedure. In Fig. 8(B), 250 s, 200 s, and 30 s hemostatic time were noted for MCMG3, MHMG3, and MHCMG7 respectively, which clearly showed 6.6 times increased hemostatic ability of MHCMG7. From Table 4, it is
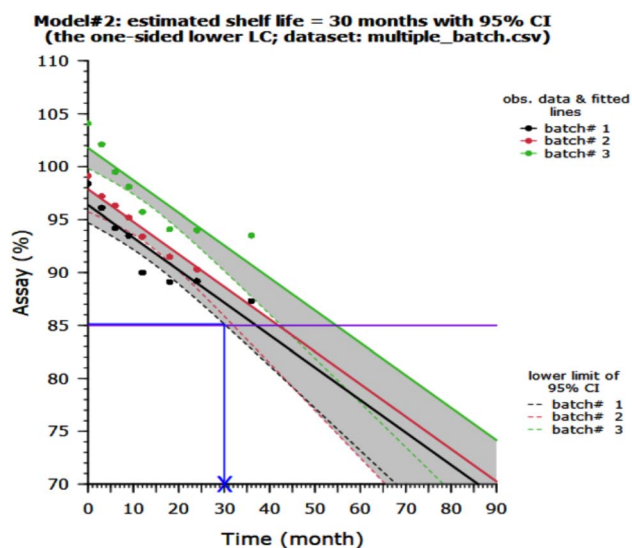
Table 3 GC loaded MHMG3, MCMG3, and MHCMG7 release profile and entrapment efficiency with application of various kinetic release models

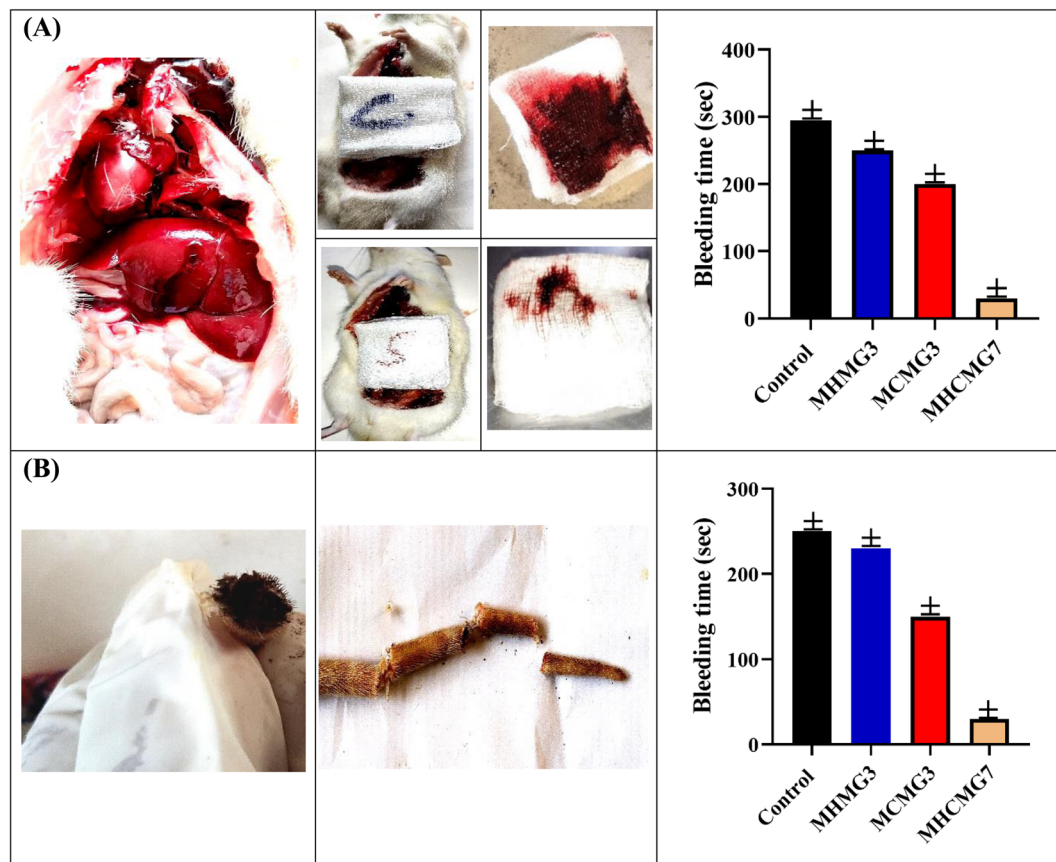| Formulations	Zero-order kinetics		First order kinetics		Higuchi's model		Korsmeyer–Peppas model	
	K_0 (h^{-1})	R^2	K_1 (h^{-1})	R^2	K_H (h^1)	R^2	n	R^2
MHMG3	7.259	0.8371	0.145	0.9978	22.539	0.9740	0.492	0.9698
MCMG3	9.85	0.4298	0.264	0.9508	28.056	0.9665	0.548	0.9442
MHCMG7	6.062	0.2498	0.236	0.8884	23.799	0.9729	0.310	0.9846

Fig. 8   (A) Rat liver laceration test showing improved clotting and hemostatic ability of MHCMG7 than MHMG3 and MCMG3, while in part (B) rat tail amputation test with bleeding time is shown.

Table 4   Effect of gemcitabine loaded different magnetic microspheres on hemostatic time and weight of whole blood clot in rat liver laceration and rat tail amputation test

Gemcitabine loaded formulation	Haemostasis time (s)	Whole blood clot weight (mg)	Rat liver laceration (weight of blood g)	Rat tail amputation (weight of blood g)
Control	232 ± 6.08	82.4 ± 5.08	3.33 ± 0.03	1.33 ± 0.03
MHMG3	147 ± 5.93	144.7 ± 4.99	1.35 ± 0.03	1.02 ± 0.03
MCMG3	216 ± 6.08	216.2 ± 5.04	1.26 ± 0.03	1.00 ± 0.03
MHCMG7	89 ± 7.13	194.6 ± 5.99	0.03 ± 0.001	0.50 ± 0.003

clear that the blood weight in a gram of the control, MCMG3, MHMG3, and MHCMG7 are 1.330, 1.020, 1.000, and 0.500, respectively. Similar findings were also mentioned in our previous work by Hanif *et al.*[14]

3.7.   Histopathological studies

Different stages of colorectal cancer development and therapeutic effects are shown in Fig. 9(A)–(H). The formulation of MHCMG7MM showed the best results and rapid development of normal colon cells as compared to the gemcitabine reference formulation. A moderate-to-mild intracellular positive response was observed in glass slides from the MM. The positive reaction was responded to the dose of gemcitabine loaded in MHCMG7. Different stages of development and treatment of colorectal

cancer are shown in Fig. 9(A)–(H). The number of aberrant crypt foci (ACF) was measured after a different period and an increased ACF number was found in Fig. 9(A)–(D) due to dimethylhydrazine. Well-differentiated glandular adenocarcinoma tissue is shown in the image in Fig. 9(A) and (B), while poorly differentiated glandular adenocarcinoma homogeneous tissue is observed in the image in Fig. 9(C) and (D). Fig. 9(E)–(H) shows the schematic regeneration of normal body cells after therapy with GC-loaded MHCMG7MM for up to 12 weeks. Dense stroma image patches cluster to loose stroma clusters were observed during the development of normal body cells.[53] Healing of mucosa, regeneration of epithelial cells, and recovery from colorectal cancer were successfully investigated by histopathological examination.
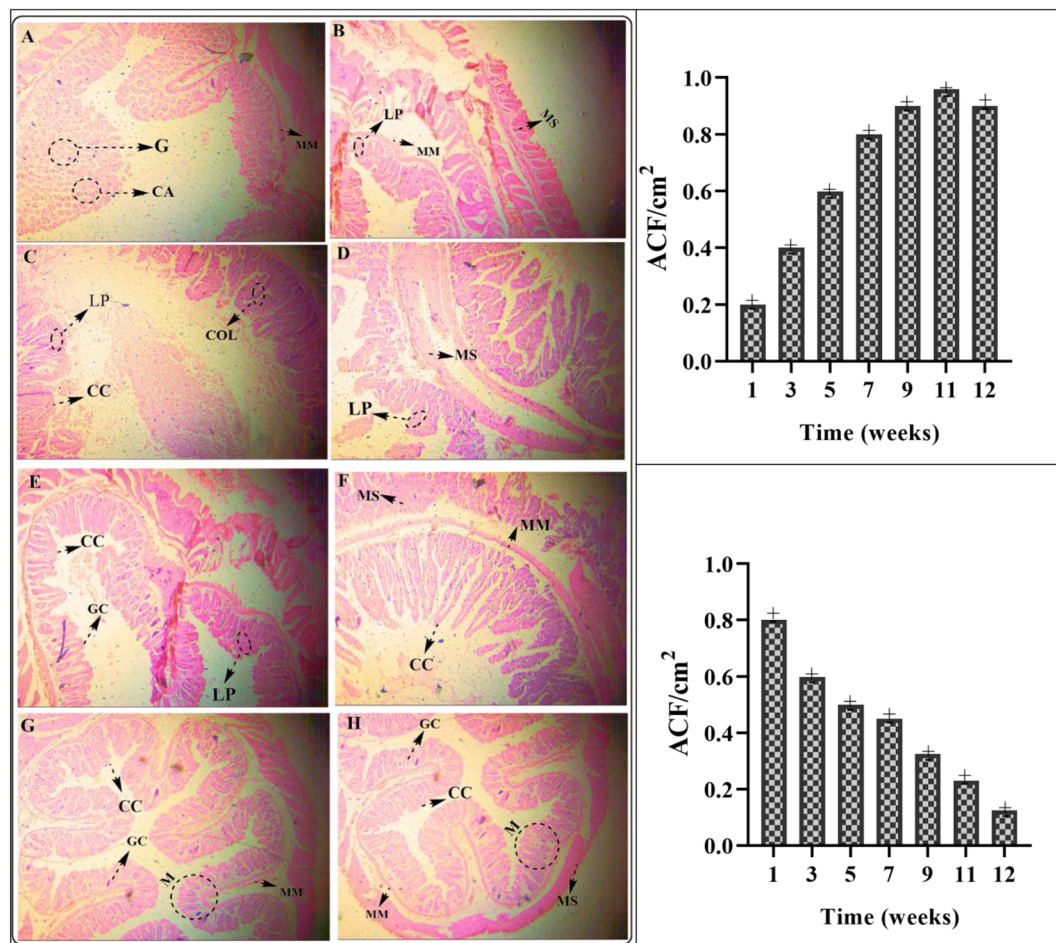
Fig. 9 Different stages of development and treatment of colorectal cancer from image (A) to (H). The number of aberrant crypt foci (ACF) per cm^2, granulomas (G), and crypt abscesses (CA) were measured after a different period and an increase in ACF number is found in (A) to (D) due to dimethylhydrazine. Well-differentiated granuloma (G) tissue is shown in (A) and (B) while poorly differentiated glandular adenocarcinoma homogeneous tissue is observed in (G) and (H). (E) to (H) show the schematic of the regeneration of normal body cells after therapy with GC-loaded MHCMG7 magnetic microspheres for up to 12 weeks. (LP: lamina propria, MM: muscularis mucosa, MS: muscularis, CC: columnar cells, COL: crypts of Lieberkühn, GC: goblet cells).

3.8. Cell viability study and safety profile

The resazurin assay was used to determine the cytotoxic activity of biological materials in formulation MHCMG7, as shown in Fig. 3(D).[25] For positive control MEM, MHCMG7 (0.5%), MHCMG7 (1.0%), and negative control (Triton X-100), respectively, the percentage viability was 99, 96, 94, and 0%. The findings demonstrated that MCMG3 produced superior outcomes and served as an essential medium for the growth of Caco-2 cells, while MHMG3 also improved epithelial cell regeneration and produced results that were within acceptable limits. However, the two together improved cell development because CTS provided more nutrients. In contrast to MCMG3 and MHMG7, MHCMG7 demonstrated greater biocompatibility, biodegradability, and enhanced cell regeneration. As a negative control, Triton X-100 eliminated all the Caco-2 cells. Fig. 3(D) used absorbance measurements collected at 3 and 24 h intervals to calculate the percentage viability of MHCMG7 (0.5%) and MHCMG7 (1.0%).[54]

The biocompatibility and biodegradability of natural polymer chitosan and clay halloysite nanotubes were considered safe for use. Target drug delivery of MM also minimized the toxic effect of carcinogenic drugs. The chitosan-coated halloysite MM is widely used in biomedical applications due to its therapeutic effect on carcinogenic colorectal hemorrhage.[54]

4. Conclusion

Treatment of carcinogenic hemorrhage can be possible using the developed controlled-release (CR) strategy of GC. Synthesized CR and targeted release of GC-containing magnetic microspheres (MM) of halloysite nanotubes (MHMG), chitosan (MCMG), and their combination (MHCMG) by co-emulsion techniques proved a good alternative to intravascular use of GC. The spherical shape of CTS microspheres and the irregular shape of HNT microspheres proved to be better solution for oral drug delivery of GC. The combination of both HNT and CTS microspheres made them more targeted in case of optimized

MHCMG7 formulation. Decreased hemostatic time and whole blood clotting time with the regeneration of epithelial cells are more applicable in general and in cancerous patients. Magnetic microspheres can be considered a carrier for the release of anticancer drugs. In the future perspective, MHCMG7 magnetic microspheres loaded with GC may be applied for various cancers such as breast cancer and bladder cancer along with radiotherapy respectively.

Abbreviations

GC	Gemcitabine
CTS	Chitosan
$FeCl_3 \cdot 6H_2O$	Iron(III) hydrochloride hexahydrate
$FeCl_2 \cdot 4H_2O$	Iron(II) hydrochloride tetrahydrate
MM	Magnetic microsphere
HNTs	Halloysite nanotubes
MHMG	Magnetic microspheres of HNTs
MCMG	Magnetic microspheres of CTS
MHCMG	Magnetic microspheres of HNTs and CTS
VSM	Vibrating sample magnetometer
XRD	X-Ray diffraction
EDS	Energy dispersive spectroscopy
SEM	Scanning electron microscopy
FTIR	Fourier transform infrared spectroscopy
TGA	Thermogravimetric analysis
CRC	Colorectal cancer
BMI	Body mass index
GIT	Gastrointestinal tract
CTS	Chitosan
HEPES	4-(2-hydroxyethyl)-1-piperazineethanesulfonic acid
PPD	*para*-phenylenediamine
KH_2PO_4	Sodium tetraborate, potassium dihydrogen phosphate
GST	Glutaraldehyde saturated toluene
aPTT	Activated partial thromboplastin time
PTT	Prothrombin test
ACF	Aberrant crypt foci
ACF	Aberrant crypt foci

Ethical statement

All animal procedures performed in accordance with guidelines for care and use of laboratory animals of Bahauddin Zakariya University and experiments were approved by the animal Ethical Committee of Faculty of Pharmacy, Bahauddin Zakariya University, Multan.

Author contributions

Muhammad Hanif was the supervisor of all experiments. Khalid Mahmood was the supplier of chemicals and reagents. The writer, reviewer, and critical analyzer were Muhammad Qaiser and Dure Shahwar. Sajid Majeed and Muhammad Qaiser was the analyst that perform the analysis of formulation and *in vivo* activities. Muhammad Harris Shoaib was the scientist who develop the chemical reaction. Ghulam Abbas and Nabeela Ameer help with manuscript writing.

Conflicts of interest

The authors report no conflicts of interest. The authors alone are responsible for the content and writing of this article.

References

1 C. Dai, C. Liu, J. Wei, H. Hong and Q. Zhao, *Biomaterials*, 2010, **31**, 7620–7630.

2 R. De Silva, P. Pasbakhsh, K. Goh, S.-P. Chai and H. Ismail, *Polym. Test.*, 2013, **32**, 265–271.

3 S. Kakar, D. Batra, R. Singh and U. Nautiyal, *J. Acute Dis.*, 2013, **2**, 1–12.

4 S. Kiralp, A. Topcu, G. Bayramoğlu, M. Y. Arıca and L. Toppare, *Sens. Actuators, B*, 2008, **128**, 521–528.

5 A. Pich, S. Bhattacharya, H. J. P. Adler, T. Wage, A. Taubenberger, Z. Li, K. H. van Pee, U. Böhmer and T. Bley, *Macromol. Biosci.*, 2006, **6**, 301–310.

6 G. Cavallaro, L. Chiappisi, P. Pasbakhsh, M. Gradzielski and G. Lazzara, *Appl. Clay Sci.*, 2018, **160**, 71–80.

7 L. Lisuzzo, G. Cavallaro, S. Milioto and G. Lazzara, *Polym*, 2020, **12**, 1766.

8 L. Lisuzzo, G. Cavallaro, S. Milioto and G. Lazzara, *J. Colloid Interface Sci.*, 2022, **608**, 424–434.

9 L. Lisuzzo, G. Cavallaro, S. Milioto and G. Lazzara, *Appl. Clay Sci.*, 2021, **213**, 106231.

10 J. Yao, Q. Wang, Y. Wang, Y. Zhang, B. Zhang and H. Zhang, *Desalin. Water Treat.*, 2015, **55**, 1293–1301.

11 Q. Li, T. He, Y.-Q. Zhang, H. Wu, J. Liu, Y. Qi, Y. Lei, H. Chen, Z. Sun and C. Peng, *ACS Sustainable Chem. Eng.*, 2019, **7**, 17039–17046.

12 K. Pandi, N. Viswanathan and S. Meenakshi, *Int. J. Biol. Macromol.*, 2019, **132**, 600–605.

13 H. Eskandarloo, M. Arshadi and A. Abbaspourrad, *ACS Sustainable Chem. Eng.*, 2018, **6**, 14561–14573.

14 M. S. Arshad, M. Qaiser, K. Mahmood, M. H. Shoaib, N. Ameer, N. Ramzan, M. Hanif and G. Abbas, *Int. J. Biol. Macromol.*, 2022, 314–323.

15 C. J. Ward, M. DeWitt and E. W. Davis, *ACS Appl. Nano Mater.*, 2012, 209–238.

16 M. S. Englehart, S. D. Cho, B. H. Tieu, M. S. Morris, S. J. Underwood, A. Karahan, P. J. Muller, J. A. Differding, D. H. Farrell and M. A. Schreiber, *J. Trauma Acute Care Surg.*, 2008, **65**, 884–892.

17 W. Ma, J. Dai, X. Dai, Z. Da and Y. Yan, *Desalin. Water Treat.*, 2016, **57**, 4162–4173.

18 Q. Wang, J. Zhang, B. Mu, L. Fan and A. Wang, *Carbohydr. Polym.*, 2014, **102**, 877–883.

19 E. Türkeș and Y. Saǧ Açıkel, *Int. J. Environ. Sci. Technol.*, 2019, **17**, 1281–1294.

20 W. Zhang, C. Hou, Y. Li, Q. Zhang and H. Wang, *J. Colloid Interface Sci.*, 2020, **558**, 115–122.

21 Z. Sohrabijam, A. Zamanian, M. Saidifar and A. J. P. M. S. Nouri, *Colloids Surf., B*, 2015, **11**, 282–286.

22 L. Sun, Y. Chen, Y. Zhou, D. Guo, Y. Fan, F. Guo, Y. Zheng and W. Chen, *Asian J. Pharm.*, 2017, **12**, 418–423.

23 J. Lee and H. Sah, *Pharmaceutics*, 2022, **14**, 1540.

24 V. Shekhovtsov, *Glass Ceram.*, 2022, **79**, 282–286.

25 S. Anoopkumar-Dukie, J. Carey, T. Conere, E. O'sullivan, F. Van Pelt and A. Allshire, *Br. J. Radiol.*, 2005, **78**, 945–947.

26 T. Kaur, S. Kaur and P. Kaur, *Int. J. Appl. Pharm.*, 2017, **9**, 60–65.

27 M. Liu, Y. Shen, P. Ao, L. Dai, Z. Liu and C. Zhou, *RSC Adv.*, 2014, **4**, 23540–23553.

28 N. P. Du Sert, A. Ahluwalia, S. Alam, M. T. Avey, M. Baker, W. J. Browne, A. Clark, I. C. Cuthill, U. Dirnagl and M. Emerson, *PLoS Biol.*, 2020, **18**, e3000411.

29 R.-R. Yan, D. Xue, C. Su, Y. Xu, J.-S. Gong, Y.-L. Liu, M. Jiang, Y. Geng, G.-Z. Lv and Z.-H. Xu, *Colloids Surf., B*, 2022, **218**, 112770.

30 C. Zheng, J. Liu, Q. Bai, Y. Quan, Z. Li, W. Chen, Q. Gao, Y. Zhang and T. Lu, *Mater. Des.*, 2022, 111116.

31 A. E. Rogers, B. J. Herndon and P. M. Newberne, *Cancer Res.*, 1973, **33**, 1003–1009.

32 H. Yoshida, T. Shimazu, T. Kiyuna, A. Marugame, Y. Yamashita, E. Cosatto, H. Taniguchi, S. Sekine and A. Ochiai, *J. Gastrointest. Cancer*, 2018, **21**, 249–257.

33 S. Sharif, G. Abbas, M. Hanif, A. Bernkop-Schnürch, A. Jalil and M. Yaqoob, *Colloids Surf., B*, 2019, **184**, 110527.

34 E. Türkeș and Y. S. Açıkel, *Int. J. Environ. Sci. Technol.*, 2020, **17**, 1281–1294.

35 S. J. Luo, P. Zhang, Y. A. Mei, J. B. Chang and H. Yan, *J. Appl. Polym. Sci.*, 2016, **133**, 1–5.

36 P. Podzus, M. Daraio and S. Jacobo, *Phys. B*, 2009, **404**, 2710–2712.

37 G.-y. Li, Y.-r. Jiang, K.-l. Huang, P. Ding and J. Chen, *J. Alloys Compd.*, 2008, **466**, 451–456.

38 M. Parsian, G. Unsoy, P. Mutlu, S. Yalcin, A. Tezcaner and U. Gunduz, *Eur. J. Pharmacol.*, 2016, **784**, 121–128.

39 A. Molaei, A. Amadeh, M. Yari and M. R. Afshar, *Mater. Sci. Eng., C*, 2016, **59**, 740–747.

40 S. Dhawan, A. K. Singla and V. R. Sinha, *AAPS PharmSciTech*, 2004, **5**, 122–128.

41 E. M. Rodrigues, N. D. Calvert, J. C. Crawford, N. Liu, A. J. Shuhendler and E. Hemmer, *Small*, 2022, 2107130.

42 D. Mandal, D. Sathiyamoorthy and V. G. Rao, *Fusion Eng. Des.*, 2012, **87**, 7–12.

43 X. Xiong, Y. Wang, W. Zou, J. Duan and Y. Chen, *J. Chem.*, 2012, **2013**, 1–8.

44 L. Chyiy and M. Saravanan, *Int. J. Pharm. Pharm. Sci.*, 2015, **7**, 203–206.

45 Y. Xie, D. Qian, D. Wu and X. Ma, *J. Chem. Eng.*, 2011, **168**, 959–963.

46 P. Luo, Y. Zhao, B. Zhang, J. Liu, Y. Yang and J. Liu, *Water Res.*, 2010, **44**, 1489–1497.

47 P. R. Chang, J. Yu, X. Ma and D. P. Anderson, *Carbohydr. Polym.*, 2011, **83**, 640–644.

48 N. Devi and J. Dutta, *Int. J. Biol. Macromol.*, 2019, **127**, 222–231.

49 M. Kim, S. C. Jee, J.-S. Sung and A. A. Kadam, *Int. J. Biol. Macromol.*, 2018, **118**, 228–237.

50 R. Kamble, M. Ghag, S. Gaikawad and B. K. Panda, *J. Adv. Sci. Res.*, 2012, **3**, 25–29.

51 H. Hosseinzadeh, F. Atyabi, R. Dinarvand and S. N. Ostad, *Int. J. Nanomed.*, 2012, **7**, 1851.

52 C. Kilkenny, W. J. Browne, I. C. Cuthill, M. Emerson and D. G. Altman, *J. Pharmacol. Pharmacother.*, 2010, **1**, 94–99.

53 B. S. Reddy, Y. Hirose, R. Lubet, V. Steele, G. Kelloff, S. Paulson, K. Seibert and C. V. Rao, *Cancer Res.*, 2000, **60**, 293–297.

54 P. Venkatesan, N. Puvvada, R. Dash, B. P. Kumar, D. Sarkar, B. Azab, A. Pathak, S. C. Kundu, P. B. Fisher and M. Mandal, *Biomaterials*, 2011, **32**, 3794–3806.